Heat transfer simulation for continuous Laser and GTA welding of 22MnB5 steel thin structure

Intissar FRIH[1]*, Alexandre MATHIEU[1], Sadok GAIED[2]

1 Laser and Materials Treatment of ICB laboratory, UMR 6303 CNRS / University of Bourgogne IUT Le Creusot - 12, rue de la Fonderie – 71200 Le Creusot
2 Multimaterials & Assembly Research Group ArcelorMittal, Global Research and Development Montataire, BP 30109 - 1, route de Saint Leu, F-60761 Montataire Cedex.

*(Corresponding author: Intissar.FRIH@u-bourgogne.fr)

Abstract - In this study, both equivalent heat sources due to continuous Laser and GTA (Gas Tungsten Arc) welding are identified. Three-dimensional thermal simulations model has been proposed and applied to 22MnB5 steel thin plates. The solved model provides the temperature fields and therefore the molten zone shape. Both equivalent heat sources have been adjusted according to thermocouple temperature measurements and macrographic cross-section observation. A good agreement between the predicted temperature and the experimental thermocouple measurements has been found.

Keywords: heat source, numerical simulation, thin plate, GTA welding, Laser welding.

Nomenclature

ρ	density, kg/m^3	T	temperature, °C
C_p	specific heat capacity, J/kg.°C	h_c	heat transfer coefficient, W/m².°C
k	thermal conductivity, W/m.°C	ε	thermal emissivity coefficient.

1. Introduction

Welding is one of the joining technologies the most used in the fabrication industry, such as automobile, offshore structures. However, during welding, the heat input and the cooling rate may cause a modification of the microstructure and the appearance of the residual stress in the weld metal [1].

Before determining the residual stress distribution in the welded thin plate, it is necessary to propose a heat source model and to validate it by comparing with experimental temperature measurements.

In the present work, Laser welding (LW) and GTA welding have been studied. In simulation, it is of utmost importance to correctly choose and identify a welding heat source to predict precisely the temperature distribution in the welded plates.

A double ellipsoidal model proposed by Goldak et al. [2] was commonly used for arc welding in numerical simulation whose parameters are calculated from experimental observations of the molten pool [3, 4]. For Laser butt-welding, Chukkan et al. found that the 3D conical with cylindrical shell heat source model predicted well the induced thermal cycles and residual stresses [5, 6]. Both models have been chosen and used, respectively, for Laser welding and GTA welding in finite elements models.

https://doi.org/10.25855/SFT2020-019

2. Experimental details

The base material is a low-alloy steel 22MnB5 which is provided by ArcelorMittal group. The chemical composition of the 22MnB5 is given in Table 1 [7]. The thermal material properties as a function of temperature are listed in Table 2 [8].

The size of the sample is 100 mm×100 mm×1.5 mm. Two specimen have been welded, one by LW and the other by GTA welding without addition of a filler wire. For LW, the laser power is 5.2 kW, the welding speed was 6 m/min, the focusing length is 200 mm and the shielding gas is Argon with a flow rate of 20 L/min. For GTAW, the average voltage U is 14 V, the average current I is 281 A, the welding speed is 1.2 m/min and the shielding gas is, also, pure Argon with a flow rate of 15 L/min.

As shown in Figure 1, ten K-type thermocouples with 0.1 mm diameter have been arc-discharge welded to bottom surface of the welded plate in order to measure temperatures developing during welding.

To visualize the melt pool shape, a high-speed camera has been used for recording the welding process. The Phantom V9.1 camera is capable to record 500 frames per second.

	C%	Mn%	P%	Si%	Cr%	S%	Al%	B%	Ti%
22MnB5	0.23	1.22	0.013	0.21	0.2	0.002	0.041	0.0027	0.032

Table 1: *Chemical composition for 22MnB5 steel*

T [°C)]	20	100	200	300	400	500	600	700
ρ [kg/m^3]	7900	7830	7822	7800	7750	7700	7650	7600
Cp [J/kg°C]	470	480	510	540	575	640	700	750
k [W/m°C]	39.0	42.5	43.5	45.0	46.5	48.0	50.5	57.5

Table 2: *Thermal material properties for 22MnB5 steel*

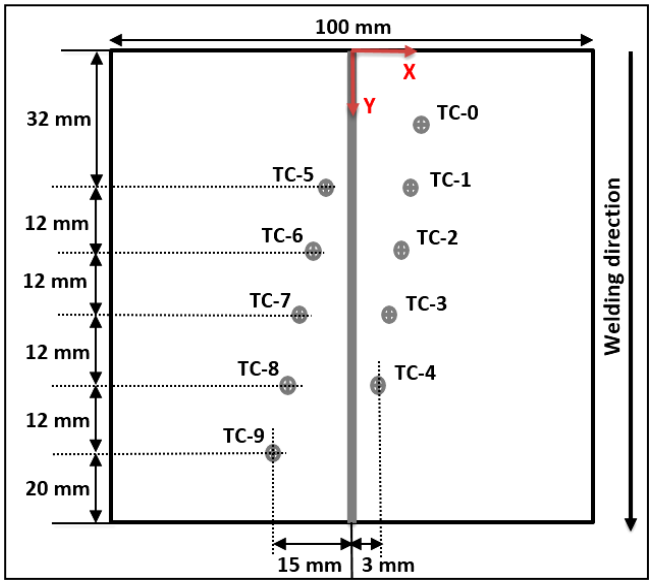

Figure 1: *Positioning of thermocouples (bottom view)*

3. Numerical procedure

In the present study, heat transfer analysis has been performed by developing a full three-dimensional (3-D) finite element model with moving heat source.

3.1. Finite element model

For modeling of a welding procedure, the finite element method FEM based software ABAQUS 6.18 has been used. As shown in Figure 2, the 3-D model has been performed in order to validate the thermocouples temperature measurements. The thermal material properties as a function of temperature have been used for present simulation. The mesh has been built using the 8-node convection/diffusion brick element type DCC3D8. In order to resolve the high temperature gradient, finer meshes have been designed at the fusion zone and its vicinity. However, the mesh size has been increased progressively with the distance from the weld center in order to reduce computational time. In the model, total number of nodes is 101 718, and total number of meshes is 88 200.

The temperature values during welding process at each node were computed by using a non-linear isotropic Fourrier heat flux equation [8]:

$$\rho(T)c_p(T)\frac{\partial T}{\partial t} = k(T)\left[\frac{\partial}{\partial x}\left(\frac{\partial T}{\partial x}\right) + \frac{\partial}{\partial y}\left(\frac{\partial T}{\partial y}\right) + \frac{\partial}{\partial z}\left(\frac{\partial T}{\partial z}\right)\right] + q(x,y,z) \quad (1)$$

where $q(x,y,z)$ is the internal heat source (W/m^3), t is the time (s) and x, y, z are coordinates in the reference system (m). The initial temperature was noted as 20°C, the heat convection is considered by an effective heat transfer coefficient h_c = 25 W.m^{-2}.K^{-1} and a thermal emissivity coefficient ε = 0.69 which are adjusted to reproduce the characteristics of the melted zone.

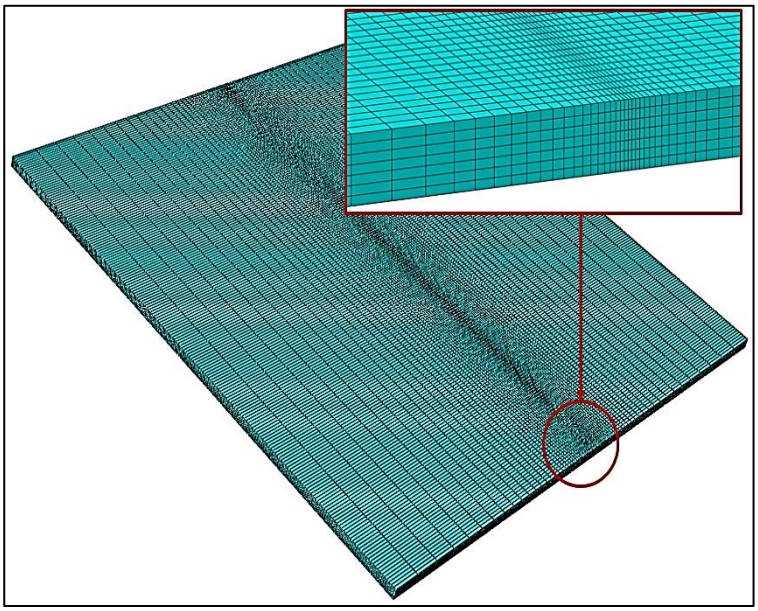

Figure 2: *Mesh of three-dimensional model*

3.2. Heat source design

In this research, both identified heat sources for Laser welding and GTA welding have been written in simplified FORTRAN code, which takes into account all the parameters identified experimentally.

3.2.1. In laser beam welding

The weld geometry has been given by metallographic observation as shown in Figure3. The geometry can be simplified as a "V" combined with an "U" shapes. The parameters describing a weld shape are presented in Table 3.

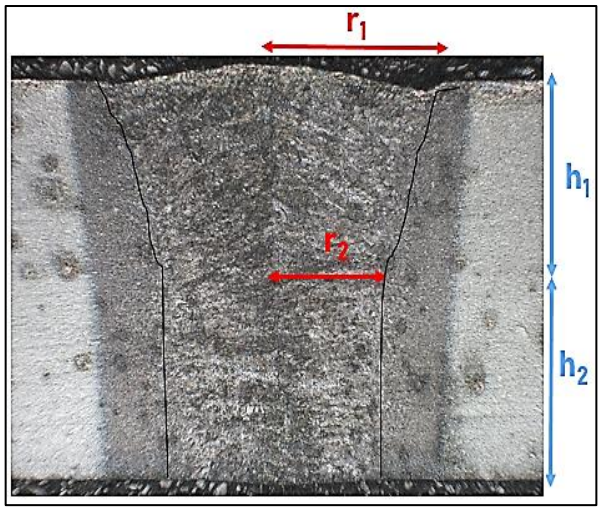

Figure 3: *Macrograph with fusion line boundary (Laser welding)*

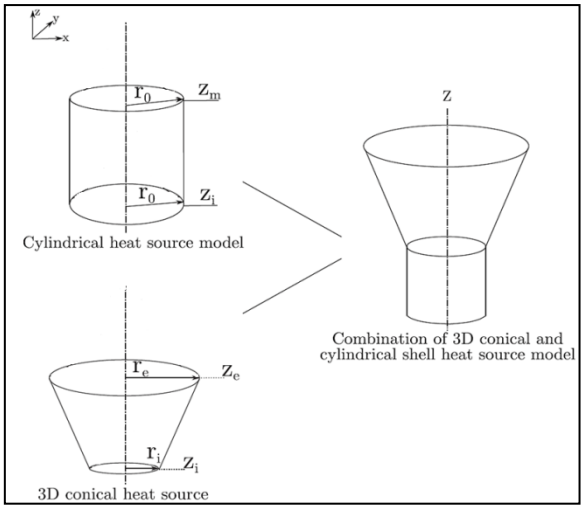

Figure 4: *Schematic diagram of a cylindrical shell heat source* [5]

A 3-D conical with a cylindrical shell heat source model has been proposed in this paper. Figure 4 shows a schematic diagram of this heat source [5]. The heat flux Q in the volumetric heat source with uniform density, is expressed according to equation (2):

$$Q = \eta P / V_T \tag{2}$$

where P is the power of Laser beam, V_T is the total volume of the heat source and η is the thermal efficiency, it has been assumed to be 0.7 in this study [9]. V_T is equal to the sum of cone and cylinder volumes and can be calculated by the following expression:

$$V_T = \pi/3.(r_1^2 + r_2^2 + r_1.r_2).h_1 + \pi.r_2^2.h_2 \tag{3}$$

where $r_1, r_2, h_1 and\ h_2$ are the geometry parameters used in the combined heat source.

Parameter	r_1	r_2	h_1	h_2
Value (mm)	0.70	0.55	0.75	0.75

Table 3: *Parameters of combined heat source in laser beam welding*

3.2.2. In GTA welding

The macrograph of molten pool shape was obtained using a high-speed camera as presented in Figure 5. The heat source geometric parameters are the front length c_f, the rear length c_r, the width a, and the depth b. The measurements of the weld pool geometry have been summarized in the Table 4. Based on Figure 5, the weld pool geometry corresponds to the geometric shape of 3D Goldak heat source.

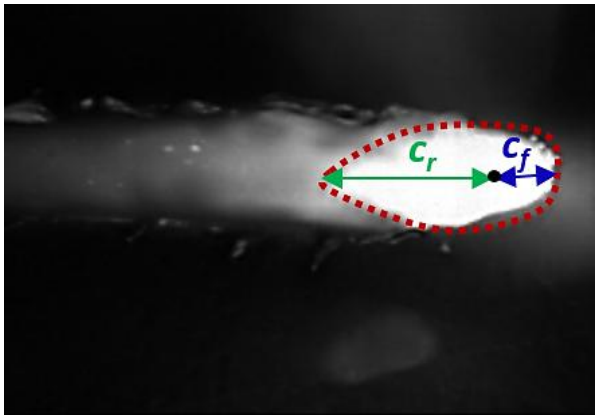

Figure 5: *Top view of Molten pool (Phantom V9.1 camera)*

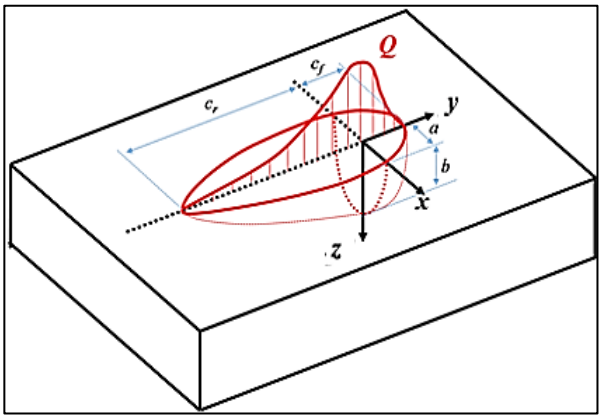

Figure 6: *Goldak's double-ellipsoid volumetric heat source* [2]

The heat flux distribution in the heat source may be expressed by the following equations:

$$q_{\mathrm{r}}(x,\ y,z) = Q.\frac{6\sqrt{3}f_r}{abc_r\pi^{3/2}}exp\ (\frac{-3x^2}{a^2})exp\ (\frac{-3y^2}{c_r^2})exp\ (\frac{-3z^2}{b^2}) \quad (4)$$

$$q_{\mathrm{f}}(x,\ y,z) = Q.\frac{6\sqrt{3}f_f}{abc_f\pi^{3/2}}exp\ (\frac{-3x^2}{a^2})exp\ (\frac{-3y^2}{c_f^2})exp\ (\frac{-3z^2}{b^2}) \quad (5)$$

$$f_r + f_f = 2 \quad (6)$$

$$Q = \eta UI \quad (7)$$

Where *x*, *y*, and *z* are the coordinates in the reference system, Q = 3174.2 W, is the net power, and η is arc efficiency was assumed to be 0.8 for GTAW [10]. Moreover, f_f is 0.46 and f_r is 1.54 represent the scaling factors in the front and rear parts, respectively.

Parameter	*a*	*b*	c_r	c_f
Value (mm)	3.0	1.5	10	2.98

Table 4: *Measurements of the weld pool geometry*

4. Result and discussion

4.1. Results of laser welding

Figure 7 compared the weld bead cross-section predicted by finite element model and that obtained during Laser welding. The 22MnB5 steel melts at around 1510°C. The simulated results matches the measurements in Laser welded joint. The FEM predicted shape and size of fusion zone are similar to those obtained by experiments. Therefore, the overall shape of Laser welded joint is matching exactly when using a 3-D conical with cylindrical shell heat source model.

The validation of heat source model has been completed by a comparison of thermal cycle results. Figures 8, 9 an 10 show thermal cycle predicted by finite element model and that obtained using three thermocouples TC-1, TC-3 and TC-4 respectively. A good matching in profile is observed.

The peak temperature value predicted by the model presents a small difference, i.e. below 10°C. Moving away from the fusion line, the temperature drop very speedily across the weld. This showed that the temperature gradients are very high around the fusion zone in Laser welding.

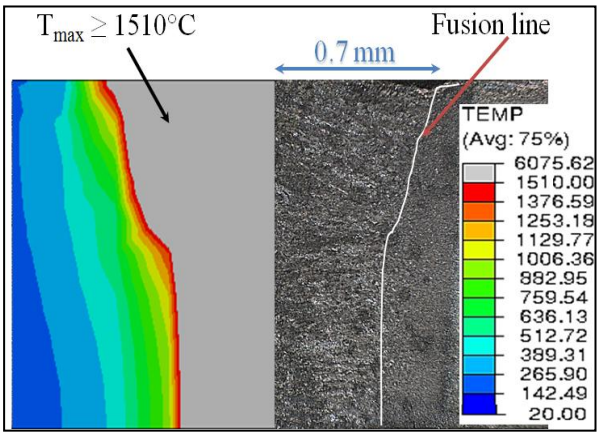

Figure 7: *Comparison of LW fusion zone between FEM and experiment.*

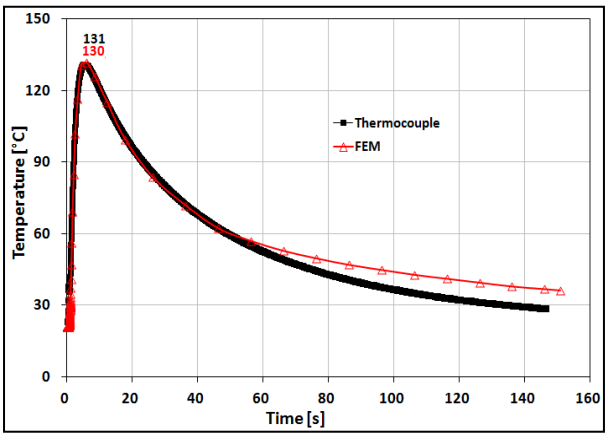

Figure 8: *Thermal cycle comparison in FEM results and thermocouple TC-1 measurements.*

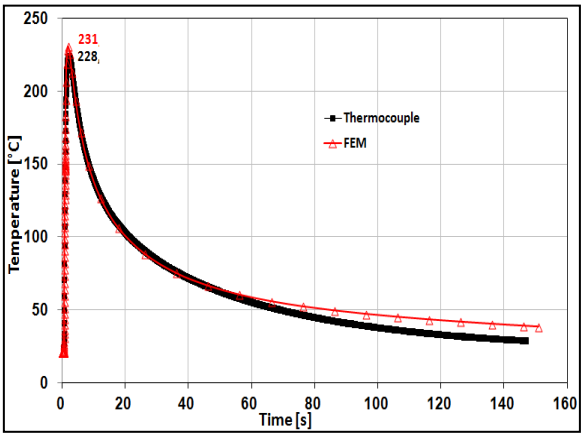

Figure 9: *Thermal cycle comparison in FEM results and thermocouple TC-3 measurements.*

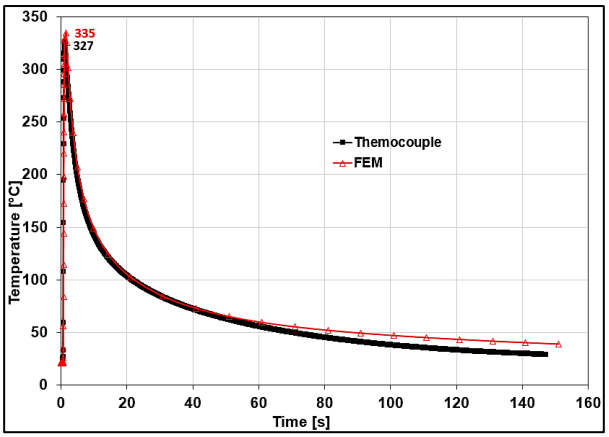

Figure 10: *Thermal cycle comparison in FEM results and thermocouple TC-4 measurements.*

4.2. Results of GTA welding

The comparison of the geometries of the molten zones with experimental observation appears to validate the model of a thermal source without additional adjustment (see Figure 11).

Comparing Figure 7 and Figure 11, it can be seen that the fusion zone due to Laser welding (1.4 mm) is much smaller than that induced by GTA welding (6 mm).

Figure 12, 13 and 14 compare the thermal cycles given by finite element results and that obtained using three thermocouples TC-3, TC-5 and TC-7 respectively. Therefore, the numerical model is matching exactly when using a Goldak type double-ellipsoid volumetric heat source.

However, a small difference has been observed at lower temperature, during cooling and it may be caused by the formation of a martensitic structure in the welded zone due to higher cooling rate, which is not taken into account in the actual numerical model.

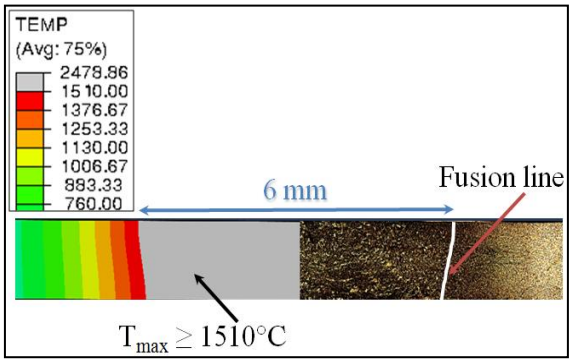

Figure 11: *Comparison of GTAW fusion zone between FEM and experiment.*

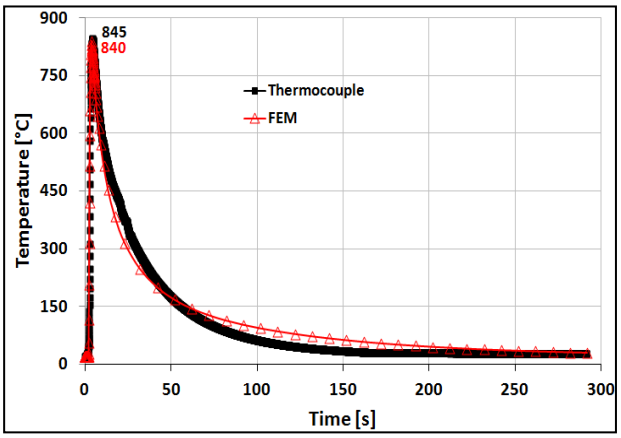

Figure 12: *Thermal cycle comparison in FEM results and thermocouple TC-3 measurements.*

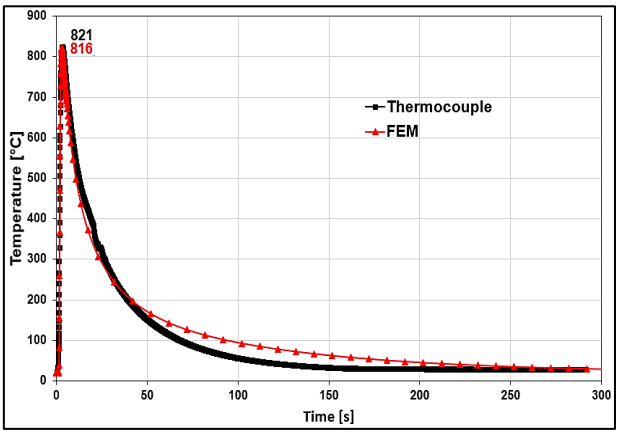

Figure 13: *Thermal cycle comparison in FEM results and thermocouple TC-5 measurements.*

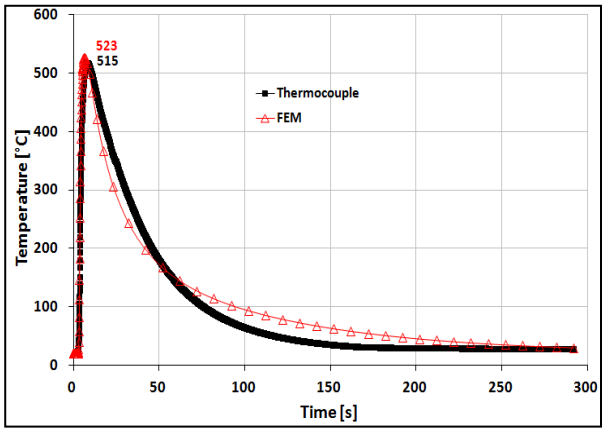

Figure 14: *Thermal cycle comparison in FEM results and thermocouple TC-7 measurements.*

5. Conclusion

In the present research, two 3D models of heat transfer have been developed to analyze laser and Gas Tungstun Arc welding respectively. For both models, the equivalent heat source parameters have been determined using the experimental results and adjusted to reproduce the characteristics of the melted zone. Numerical results have a good agreement with experimental measurements in terms of temperature distribution and weld bead shape and size. These results validate the choice of equivalent heat sources for the two welding types.

Equivalent heat sources identification is the preliminary work, final aim of this work is to introduce temperature fields obtained by thermal model into a mechanical model in order to predict residual stresses induced by welding processes.

References

[1] I. Frih, G. Montay, P.-A. Adragna, *Microstructure, hardness, and residual stress distributions in T-joint weld of HSLA S500MC steel*, *Metall. Mater. Trans. A*, 48 (2017), 1103–1110.

[2] J. Goldak, A. Chakravarti, M. Bibby, *A new finite element model for welding heat sources. Metall Mater Trans B-Proc Metall Mater Proc Sci* (1984), 15B:299–305.

[3] S. Joshi, J. Hildebrand, A. S. Aloraier, T Rabczuk, *Characterization of material properties and heat source parameters in welding simulation of two overlapping beads on a substrate plate*, *Computational Materials Science*, 69 (2013), 559-565.

[4] T. T. Ngo, C. C. Wang, J. H. Huang, V. T. Than, *Estimating heat generation and welding temperature for gas metal arc welding process*, *Applied Thermal Engineering*, 160 (2019).

[5] J.R. Chukkan, M. Vasudevan, S. Muthukumaran, R.R. Kumar, N. Chandrasekhar, *Simulation of laser butt welding of AISI 316L stainless steel sheet using various heat sources and experimental validation, J. Mater. Process*. Technol. 219 (2015) 48–59.

[6] L.J. Nayak, G. G. Roy, *Thermocouple temperature measurement during high speed electron beam welding of SS 304*, *J. Optik*, 201 (2020).

[7] https://steelnavigator.ovako.com/steel-grades/22mnb5/ (Available online : 16/01/2019).

[8] G. KAZA, Contribution à l'étude de la Résistance Thermique de Contact et à sa modélisation à travers l'écrasement de l'interface tôle/outil dans la mise en forme à chaud de tôles d'acier, PhD of the Université Toulouse 3 Paul Sabatier, (2010).

[9] J. Sun, J. Klassen, T. Nitschke-Pagel, K. Dilger, Effects of heat source geometric parameters and arc efficiencyon welding temperature field, residual stress, and distortion in thin-plate full-penetration welds. The International Journal of Advanced Manufacturing Technology, (2018).

[10] J. Sun, X. Liu, Y. Tong, D. Deng, A comparative study on welding temperature fields, residual stress distributions and deformations induced by laser beam welding and CO2 gas arc welding. Materials and Design 63 (2014) 519–530.

Acknowledgements

The present work was funded by the project NEMESIS (ANR-17-CE08-0036) of the French National Research Agency (ANR).